Hindawi
Journal of Chemistry
Volume 2022, Article ID 4778830, 12 pages
https://doi.org/10.1155/2022/4778830

Research Article

Application of Samarium- and Terbium-Sensitized Luminescence via a Multivariate-Based Approach for the Determination of Orbifloxacin

Nessreen Al-Hashimi, Ahmed S. El-Shafie, Asmaa Jumaa, and Marwa El-Azazy

Department of Chemistry and Earth Sciences, College of Arts and Sciences, Qatar University, Doha 2713, Qatar

Correspondence should be addressed to Marwa El-Azazy; marwasaid@qu.edu.qa

Received 10 December 2021; Accepted 27 December 2021; Published 17 January 2022

Academic Editor: Liviu Mitu

A lanthanide-based optical sensor has been developed for the sensitive and reliable spectrofluorometric determination of the fluoroquinolone antibiotic orbifloxacin (ORLX). Reaction of ORLX and two lanthanide metal ions, Sm(III) and Tb(III), in aqueous buffered solution produced highly fluorescent complexes. Plackett–Burman design (PBD) was used to explore the impact of four factors, pH, temperature (Temp), contact time (CT), and metal volume (MV), on the fluorescence intensity (FI) of the produced complexes. The obtained data showed that pH was the most significant variable. A blend of pH = 5.0, MV = 2.0 mL, $T = 25^{\circ}C$, and CT = 10 min was used to achieve the maximum FI. FT-IR and Raman analyses were performed for the crystals of the as-prepared complexes. Obtained data showed shifting in most of the absorption bands, confirming the complexation of ORLX with both metal ions. Job's method showed that the stoichiometry for the reaction of ORLX with Sm(III) and Tb(III) was 1 : 1. The proposed method was validated following the ICH guidelines. Injection formulation was analyzed successfully with the developed method with high recovery (99.42–100.91%). The detection and quantification limits were 0.987 and 3.289 ng/mL for the ORLX-Sm(III) complex and 1.020 and 3.399 ng/mL for the ORLX-Tb(III) complex, respectively.

1. Introduction

Existence of pharmaceutically active compounds in aquatic systems has prompted several public health concerns [1]. Antibiotics are a major class of antimicrobials, which are commonly used for therapeutic and prophylactic purposes. With the current widespread and escalating use of antibiotics, their existence is representing a burden on the environment as well as the human health on the long run [2–4].

Fluoroquinolone antibiotics (FQs) are among the most widely produced and consumed antimicrobials. Possessing a broad spectrum of activity with good bioavailability, this large group of synthetic antibacterials is receiving an extensive interest and rapid acceptance in both human and veterinary medicine. The consumption of FQs represents a problem since they are partly metabolized and hence could be excreted in their active forms [5–8]. Existing at ultralow concentrations, the detection of these contaminants in different matrices represents a challenge.

Orbifloxacin (ORLX) is a third-generation veterinary FQ antibiotic that is commonly utilized for the treatment of persistent and recurring staphylococcal pyoderma and *Pseudomonas* infections that cause otitis. Chemically, ORLX is 1-cyclopropyl-5,6,8-trifluoro-1,4-dihydro-7-(cis-3,5-dimethyl-1-piperazinyl)-4-oxoquinoline-3-carboxylic acid, Scheme 1 [9–11]. ORLX together with other ten FQs was detected in raw wastewater. Detected concentrations were as high as 1900 ng/L for ciprofloxacin, compared to 9–170 ng/L for difloxacin, enrofloxacin, fleroxacin, moxifloxacin, norfloxacin, and ORLX [12].

Scheme 1. Chemical structure of orbifloxacin (ORLX).

To date, methods reported in the literature for the determination of ORLX include liquid chromatography with ultraviolet [12–14], fluorimetry [12, 15–17], or mass spectrometry as detection techniques [16–18]. In another approach, sequential injection analysis coupled to solid-phase spectroscopy was utilized to develop a terbium-sensitized

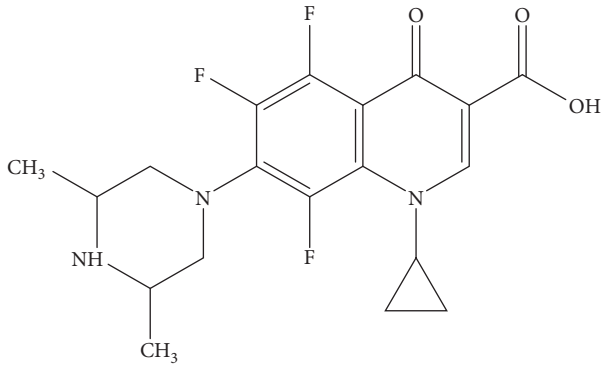

Scheme 1: Chemical structure of orbifloxacin (ORLX).

luminescent optical sensor for the analysis of ORLX in different matrices [19]. By and large, the application of chromatography in the detection of pharmaceuticals has been widely described. Yet, the need for well-trained personnel, consumption of solvents, and the sophisticated instrumentation represent major challenges.

Possessing unique luminescent characteristics when complexed with organic ligands (recognized as the antennas), lanthanide-sensitized luminescence has been recently widely described for the detection of drugs and pharmaceuticals [19–24]. Among these characteristics, the unique decay times allow an effective distinction between the background interferences in analyses. Moreover, while the uncomplexed lanthanides possess low molar extinction coefficients, the antennas serve to absorb energy at their characteristic excitation wavelength. Following the complexation, energy is transferred to the triplet state of the molecule and then to the core lanthanide ion resonance level, enhancing its luminescence intensity. Finally, radiation is emitted at the characteristic wavelength of the lanthanide ion [19–27].

To the best of our knowledge, all the reported approaches for the determination of ORLX (either chromatography or spectroscopy) were univariate-based. In such a conventional approach, one variable is studied at a time. Therefore, in addition to being time- and resource-consuming, the correlation between variables affecting the process cannot be portrayed. On the contrary, factorial design-based approaches are multivariate. In other words, all variables affecting the process are varied simultaneously, an issue that serves to reduce the number of experimental runs, use of chemicals, and consumption of resources. Moreover, the variable-variable interactions are thoroughly studied and addressed. Overall, the process is economic and green, and obtained data can be treated with a high degree of inevitability [28].

In the current approach and in continuation of our efforts for the determination of antimicrobials as per se and in formulations [29, 30], ORLX will be determined via implementing terbium [Tb(III)] and samarium [Sm(III)] ion-sensitized luminescence both as per se and in formulation. Plackett–Burman design (PBD) will be used as the multivariate optimization approach [28]. In this itinerary, four variables will be assessed, pH, temperature (Temp), reaction time (CT), and lanthanide metal volume (MV). The target will be set to maximize the fluorescence intensity (FI) as a response variable. The formed complexes will be further characterized using FT-IR, Raman, and CHN analyses. Moreover, the proposed analytical technique will be validated using the International Conference on Harmonization (ICH) guidelines in terms of linearity, sensitivity, selectivity, robustness, accuracy, and precision [31].

2. Experimental

2.1. Instruments and Software. A Shimadzu RF-6000 spectrofluorophotometer (Shimadzu Corporation, Kyoto, Japan) was used for measuring the fluorescence intensity. A quartz cell with 1.0 cm pathlength was used as a sample holder. For adjusting pH of the prepared solutions, a Jenway digital pH meter (Jenway, Staffordshire, UK) with a combined glass electrode was employed. Fourier-transform infrared radiation (FT-IR, Bruker ALPHA, Billerica, MA, USA) was used to determine the functional groups in the formed complex. The spectra were done at the range of 500–4000 cm^{-1}. The Raman spectrum of the as-prepared complex was acquired in the range of 100–3500 cm^{-1} using a DXR^{TM}2 Raman microscope (Thermo Scientific, Waltham, MA, USA), with a laser beam at 532 nm as the excitation source and 10 mW power. A CHN analyzer (FLASH 2000 CHNS/O Analyzer, Thermo Scientific, Waltham, MA, USA) was used to determine the amounts of elements in the drug alone and then in the complex. Minitab® 19 software provided by Minitab® Inc. (State College, PA, USA) was used to construct and analyze the selected experimental design.

2.2. Materials and Reagents. All reagents and chemicals were of analytical grade and were used without further purification. Ultrapure water (18.2 MΩ) was used to prepare and dilute the working solutions. ORLX was purchased from Biosynth Carbosynth® Ltd. (Compton, Berkshire, UK). Samarium(III) nitrate hexahydrate and terbium(III) chloride hexahydrate were purchased from Sigma-Aldrich (St. Louis, MO, USA). The solution's pH was adjusted to the desired value using phosphate buffer together with 0.1 M NaOH or 0.1 M HCl.

Stock solution of ORLX (5 μg/mL) was prepared by dissolving the prerequisite drug amount in deionized water. Lanthanide stock solutions were prepared by weighing respective masses of samarium(III) nitrate hexahydrate and terbium(III) chloride hexahydrate and dissolving in deionized water to give solutions which are 300 μg/mL of Sm(III) and Tb(III), respectively. Both drug and lanthanide stock solutions were freshly prepared throughout the experiments.

2.3. Preparation of the ORLX Formulation. The composition of the 'orbifloxacin injection, Victas® injection 5%, DS Pharma Animal Health Co., Ltd., Fukushima-ku, Osaka, Japan,' labelled to contain 50 mg of ORLX/mL together with 20 mg/mL of the additive benzyl alcohol was simulated. The mixture was dissolved in 100 mL deionized water. The resulting solution, 500 mg/L, was further diluted using deionized water to prepare a working solution of 5 mg/L of ORLX formulation.

2.4. Preparation of ORLX-Sm(III) and ORLX-Tb(III) Solid Samples. Solid ORLX-Sm(III) and ORLX-Tb(III) complexes were prepared by mixing 1 : 1 of ORLX and each metal solution separately. pH of the two mixtures was adjusted to 5.0 using phosphate buffer followed by stirring in a water bath at a constant temperature of 70°C and at a fixed stirring rate, 700 rpm, to prepare saturated solutions of the ORLX-lanthanide metal complex. The solutions were left to cool down, and the prepared solid samples were filtered, collected, and stored for further use. Finally, the samples were characterized using FT-IR, Raman, and CHN analyses.

2.5. General Procedure

2.5.1. Authentic Samples: Screening Phase. The investigation of the impact of four variables, pH, temperature (Temp), contact time (CT), and metal volume (MV), was studied at three levels as shown in Table 1, and the scenario was implemented as shown in Table 2.

The setup of the experimentation process consisted of a set of 16 runs, including four central points. Each sample in Table 2 was prepared by mixing 1 mL of ORLX, the specified volume of each of Sm(III) and Tb(III), followed by the addition of 1 mL of pH buffer solution. The mixture was then placed in a water bath at the assigned temperature and for the time length specified in Table 2 for each experiment. Solutions were then cooled down, and the volume was made up to the mark of 10 mL using deionized water. A blank was similarly prepared omitting ORLX. Finally, the fluorescence intensity (FI) was recorded at an excitation wavelength (λ_{ex}) of 284 nm and an emission wavelength (λ_{em}) of 458 nm against a blank.

2.5.2. Procedure for the Formulation. Aliquots of the formulation aqueous solution were transferred into 20 mL test tubes, and the scheme described under Section 2.5 was followed, however, applying the optimum conditions (direct calibration). In the same itinerary, to test the method selectivity and the impact of the formulation matrix, the standard addition method was applied. Seven samples were prepared by adding aliquots of the standard ORLX solution (final concentration of 50–300 ng/mL) to 100 ng/mL of the formulation solution and applying the optimum conditions.

2.5.3. Reaction Stoichiometry. Job's method of continuous variation [32] was used to investigate the molar ratio of the reaction of ORLX and both Sm(III) and Tb(III). Equimolar solutions (1.35×10^{-5} M) of Sm(III) and Tb(III) and the ORLX drug solutions were prepared. Series of 5.0 mL solutions were made up encompassing different proportions of both ORLX and Sm(III) and Tb(III) in separate experiments in 10 mL volumetric flasks. Phosphate buffer solution (1 mL, pH 5.0) was added to each flask, and the procedure was followed as explained under Section 2.5.

3. Results and Discussion

3.1. Spectral Characteristics. The fluorescence spectra of ORLX, Sm(III) and Tb(III), and ORLX-lanthanide are shown in Figures 1(a) and 1(b), respectively. As shown in Figure 1, Sm(III) and Tb(III) have shown a weak fluorescence emission at 440 nm when excited at 275 nm. As shown in Figure 1, the FI of both metals is very low, mainly because of the forbidden *f-f* transition. The forbidden *f-f* transition of lanthanides is responsible not only for their low absorption but also makes their direct excitation difficult, an issue which hinders their application in complicated matrices such as biological fields [33]. Yet, because of the forbidden *f-f* transitions, the relaxation from the metal excited states occurs slowly.

Table 1: Screened numerical variables and their low, mid-, and high limits.

Variables	Low (−1)	Center point (0)	High (+1)
pH (A)	5.0	6.5	8.0
Temperature, Temp (°C) (B)	25	47.5	70
Contact time, CT (min) (C)	10	50	90
Metal volume, MV (mL) (D)	0.5	1.25	2

In the same itinerary, compared to the lanthanide ions, the organic drug molecules possess a decay time on the nanosecond scale. The ORLX molecule is excited from the ground state to the singlet excited state following absorbing ultraviolet light energy. The excited molecule is then transitioned to its triplet state ($S_1 \longrightarrow T_1$) via intersystem crossing (ISC). Lastly, energy is transferred on one or many excited states of the central ion via nonradiative transition [$T_1 \longrightarrow$ Sm(III)/Tb(III)], and a strong characteristic luminescence of the core ion is emitted [22, 25]. This phenomenon is known as the 'antenna effect.' The ORLX-lanthanide complex, therefore, shows longer decay lifetimes that could extend to the microsecond scale, allowing the acquisition of well time-resolved luminescence measurements [33, 34]. As shown in Figure 1, the FI of the complex was ~15-16 times that of the metal ion and ~7 times that of ORLX.

Figure 2 shows the spectra of the ORLX-metal complex collected using increasing concentrations of ORLX ranging between 25 and 500 ng/mL.

3.2. Plackett–Burman Design (PBD)

3.2.1. Assessment of Reaction Variables. As displayed in Table 1, screening of the four variables influencing the chosen response (maximum FI), resulting from the interaction of ORLX and two lanthanides, was performed using PBD. As a multivariate approach, PBD is an efficient methodology when only the main variables are of interest [28]. The experimental scenario as prompted by PBD is revealed in Table 2. Quality tools were employed to assess the statistical significance of each independent variable on the measured response. Figure 3 shows the Pareto chart of standardized effects for the complexes of ORLX with Sm(III) and Tb(III). In both cases, pH (A) was the most statistically significant variable impacting the FI. CT (B), however, was the least significant variable in case of Tb(III) and had no effect in case of Sm(III).

Table 2: Experimental setup employing PBD.

Run no.	Point type	pH (A)	Temp (B)	CT (C)	MV (D)	FI*Sm(III)	RE**[Sm(III)]	FI ∗ Tb(III)	RE**[Tb(III)]
01	1	8.0	70.0	10	0.50	4498	0.09	3089	0.04
02	1	8.0	25.0	90	0.50	4617	0.07	3471	0.04
03	0	6.5	47.5	50	1.25	13200	0.16	17811	0.03
04	1	5.0	25.0	90	2.00	65270	0.07	47339	0.01
05	0	6.5	47.5	50	1.25	16224	0.03	17487	0.05
06	1	8.0	25.0	10	2.00	7046	0.08	5541	0.11
07	0	6.5	47.5	50	1.25	15995	0.01	16939	0.08
08	1	5.0	25.0	10	0.50	43823	0.05	44962	0.00
09	0	6.5	47.5	50	1.25	15909	0.00	17398	0.06
10	0	6.5	47.5	50	1.25	16303	0.03	19224	0.05
11	0	6.5	47.5	50	1.25	17429	0.10	17496	0.04
12	1	5.0	70.0	10	2.00	47766	0.05	45837	0.01
13	1	8.0	70.0	90	2.00	5082	0.06	3207	0.03
14	0	6.5	47.5	50	1.25	16504	0.04	19407	0.05
15	0	6.5	47.5	50	1.25	14320	0.09	18246	0.00
16	1	5.0	70.0	90	0.50	40678	0.06	41605	0.03

* FI: observed FI. ** RE: relative error = [|(observed FI − predicted FI)|/observed FI].

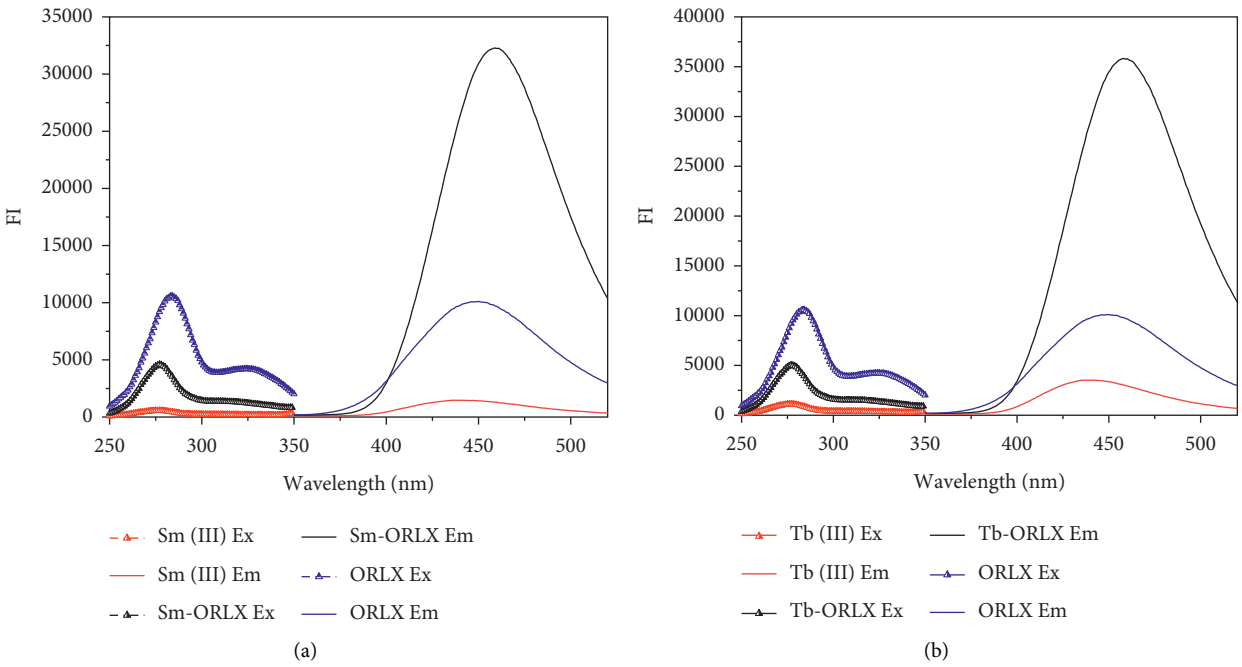

Figure 1: Excitation and emission spectra of 3 μg/ml ORLX (a) and (b), with 30 μg/ml Sm(III) (a) and 30 μg/ml Tb(III) (b), measured against a blank.

The findings of the screening phase were validated using the analysis of variance (ANOVA) at the 95.0 significance level (Table 3). As shown by the ANOVA findings, variables with a p value ˂0.05 are statistically significant, and vice versa [28]. A quick glance on the table shows that findings of ANOVA are matching completely with the Pareto charts.

3.2.2. Data Fitting and Modelling. The shown FI in both panels of Figure 3 was obtained following a Box-Cox response transformation [35] with λ (transformation factor) value = 0 and stepwise selection of terms in case of Sm(III) and $\lambda = 0.5$ with backward elimination of terms in case of Tb(III). Table 2 shows the observed values for FI as well as the RE obtained via comparing the observed responses to the model predicted values for FI. According to values of RE shown in Table 2, it is obvious that the experimental values are close to their predicted values indicating good precision for the prediction at a 95.0% confidence interval (CI).

The regression formulas, equations (1) and (2), obtained after the response transformation are shown in the following for both ORLX-lanthanide complexes, with the values of R^2, R^2-Adj (R^2-adjusted), and R^2-Pred (R^2-predicted).

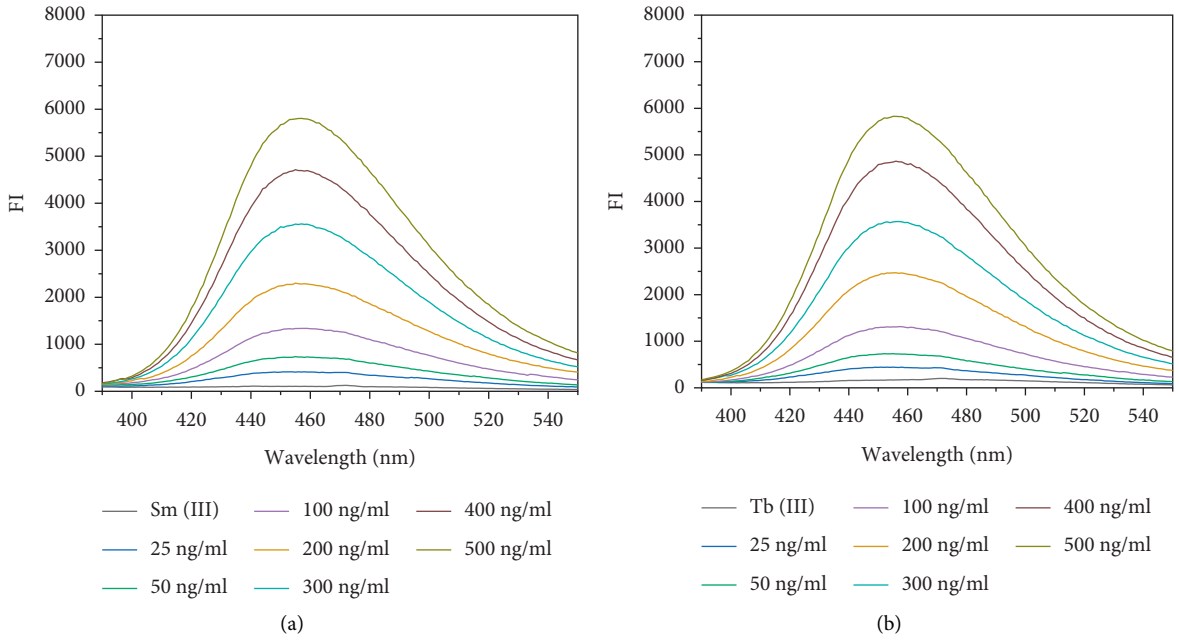

Figure 2: Fluorescence spectra for the interaction between Sm(III) (a) and Tb(III) (b) with different concentrations of ORLX from 25 to 500 ng/mL.

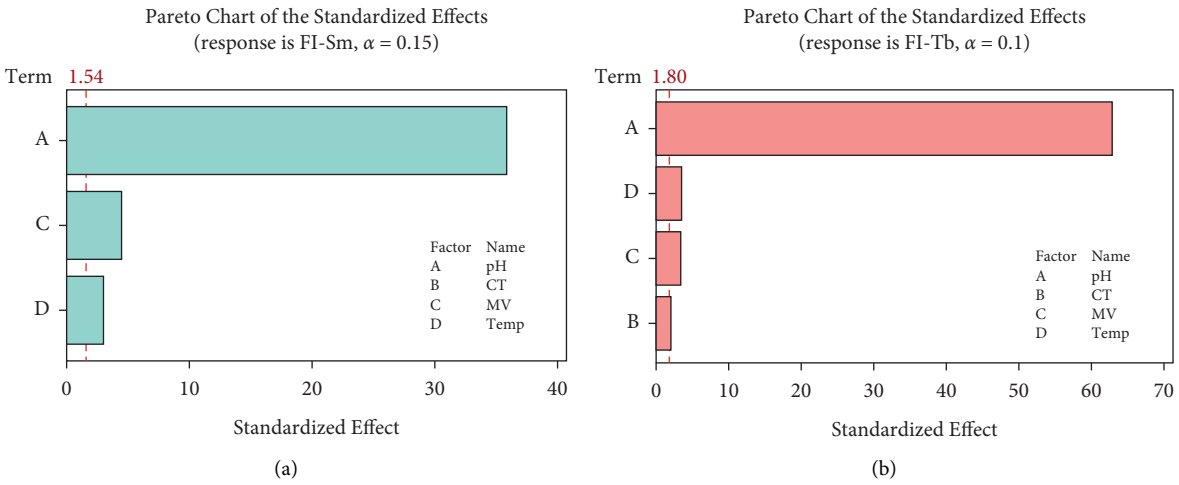

Figure 3: Pareto charts of the standardized effects for (a) ORLX-Sm(III) and (b) ORLX-Tb(III) complexes.

$$\ln(\mathrm{FI}-\mathrm{Sm}) = 14.464 - 0.7433\mathrm{pH} + 0.1840\mathrm{MV} - 0.00411\mathrm{Temp} \quad \left(R^2 = 99.10\%, R^2-\mathrm{adj} = 98.87\%, \text{ and } R^2-\mathrm{pred} = 98.23\%\right), \tag{1}$$

$$\sqrt{(\mathrm{FI}-\mathrm{Tb})} = 466.44 - 50.177\mathrm{pH} - 0.0596\mathrm{CT} + 5.37\mathrm{MV} - 0.1816\mathrm{Temp} \quad \left(R^2 = 99.73\%, R^2-\mathrm{adj} = 99.63\%, \text{ and } R^2-\mathrm{pred} = 99.36\%\right). \tag{2}$$

As shown in equations (1) and (2), the values of R^2 were high enough to indicate the goodness of fit of the proposed models. The values of R^2-Adj were in excellent agreement with R^2-Pred, demonstrating the ability of the proposed models to predict the response for a new observation. The R^2-Pred values were not markedly less than R^2, suggesting that the model was not overfit. The regression equations also show that pH has a negative influence on the FI (indicated by the negative sign).

Table 3: Analysis of variance (ANOVA) for FI of ORLX-Sm(III) and ORLX-Tb(III) complexes.

Source	DF	Adj SS	Adj MS	F value	P value
ORLX-Sm(III)					
Model	3	10.1646	3.3882	438.19	≤0.001
Linear	3	10.1646	3.3882	438.19	≤0.001
pH	1	9.9439	9.9439	1,286.04	≤0.001
MV	1	0.1523	0.1523	19.70	0.001
Temp	1	0.0684	0.0684	8.84	0.012
Error	12	0.0928	0.0077		
Curvature	1	0.0009	0.0009	0.11	0.746
Lack of fit	4	0.0369	0.0092	1.17	0.399
Pure error	7	0.0550	0.0079		
Total	15	10.2574			
ORLX-Tb(III)					
Model	4	45628.1	11407.0	997.69	≤0.001
Linear	4	45628.1	11407.0	997.69	≤0.001
pH	1	45319.2	45319.2	3963.75	≤0.001
CT	1	45.4000	45.4000	3.97	0.072
MV	1	129.800	129.800	11.36	0.006
Temp	1	133.600	133.600	11.69	0.006
Error	11	125.800	11.4000		
Curvature	1	25.5000	25.5000	2.54	0.142
Lack of fit	3	23.8000	7.90000	0.73	0.568
Pure error	7	76.5000	10.9000		
Total	15	45753.8			

DF is degrees of freedom, Adj SS is the adjusted sum of squares, and Adj MS is the adjusted mean of squares.

3.2.3. Data Optimization. Optimization of the variables obtained from the screening phase was performed using the optimization plot option in Minitab. Desirability function approach was implemented to check the accuracy of the statistical model. Optimization plot (figure is not shown) reveals that the optimum conditions for both complexes that could achieve the maximum FI were pH = 5.0, MV = 2.0 mL, $T = 25^{\circ}$C, and CT = 10 min (ORLX-Tb) with individual desirability (d) of 0.9423 and 1.000 for both Sm(III) and Tb(III), respectively. Results of the optimization phase also showed increasing pH (most statistically significant variable) and in agreement with the developed statistical models decreases the FI. This finding could be attributed to the formation of metal hydroxide at higher pH values; therefore, pH = 5.0 was used throughout the experiments [36]. Similarly, in agreement with the regression model, increasing the Temp has resulted in a slight decrease in the FI. On the contrary, increasing the MV has resulted in a slight increase in the FI.

3.2.4. Contour Plots. Contour (2D) plots were used to investigate the association between FI as a function of two factors. The darkest zone on the graph (either panel), Figure 4, shows the highest FI. For example, Figure 4(a) (FI-Sm) shows that a MV of 1.75–2.0 mL together with pH 5.0 could produce the highest FI in case of ORLX-Sm. In case of the ORLX-Tb complex (Figure 4(b)), pH ˂ 5.25 and CT of 0–80 min could produce the highest FI with a slight decrease in increasing the CT from 0 to 80 min.

3.3. Spectral Characterization of ORLX-Lanthanide Complexes

3.3.1. FT-IR Analysis. In the current approach, FT-IR was used to study the coordination of both Sm(III) and Tb(III) ions with ORLX in the formed complexes. As shown in Table 4 and Figure 5, the spectrum of ORLX shows an absorption band at 3427 cm^{-1} which could be related to the presence of either -OH stretching of carboxylic acid or N-H stretching of the secondary amine [37]. However, upon complexation with Sm(III) (Figure 5(a)), a shift to 3280 cm^{-1} occurred, and the peak was broadened as a result of forming the complex. A similar observation was noticed in case of Tb(III) complex. The C=O group also appeared in the spectrum of ORLX at 1643 cm^{-1}. νCO for ORLX was shifted following the coordination with lanthanide to 1613 cm^{-1} and 1614 cm^{-1} for both Sm(III) and Tb(III), respectively [38, 39].

Furthermore, the spectrum of ORLX showed a strong absorption band at 1278 cm^{-1}, which could be assigned to the C-N stretching of aromatic amine [40]. The νCN vibration has also shifted to 1295 cm^{-1} with the two ions. These findings confirm the complexation of ORLX with both metal ions Sm(III) and Tb(III), and they have similar coordination structures.

3.3.2. Raman Analysis. Figure 6 shows the Raman spectra of ORLX, ORLX-Sm(III), and ORLX-Tb(III) complexes. The intensity of νOH and νNH vibrations at 3091, 3082, 2940, and 2892 cm^{-1} in the ORLX spectrum has significantly decreased upon complexation with Sm(III). Moreover, these peaks appeared in ORLX-Sm(III), with a slight shift to 3084, 3014, 2940, and 2890 cm^{-1}. A similar behavior was observed in case of the ORLX-Tb(III) complex. Furthermore, a new peak for both ORLX-Sm(III) and ORLX-Tb(III) complexes appears between 3050 cm^{-1} and 3500 cm^{-1}, confirming the drug-lanthanide complexation [40–42]. The νNH vibration at 1627 cm^{-1} in the ORLX spectrum has shifted after complexation to 1638 and 1634 cm^{-1} with Sm(III) and Tb(III), respectively. Likewise, the drug's νC=C vibration at 1542 cm^{-1} appeared following the coordination at 1579 cm^{-1} for Sm(III) and 1586 cm^{-1} for Tb(III) complex. The strong vibration band νOH at 1372 cm^{-1} has shifted after the complex formation to 1394 cm^{-1} for ORLX-Sm(III) and 1397 cm^{-1} for ORLX-Tb(III), an issue that might reflect that the hydroxyl group was changed after the complexation reaction [42]. The shifts in the functional group assignments in the Raman spectra confirm the complex formation between ORLX and the two metal ions Sm(III) and Tb(III).

3.3.3. CHN Elemental Analysis. CHN analysis was used to compare the % mass of carbon, hydrogen, and nitrogen before and following complexation. As shown in Table 5, C% has significantly decreased upon complexation. A similar observation could be recorded for N% and H%. This change in the elemental composition between uncomplexed and complexed ORLX implies the formation of complex with the two lanthanides.

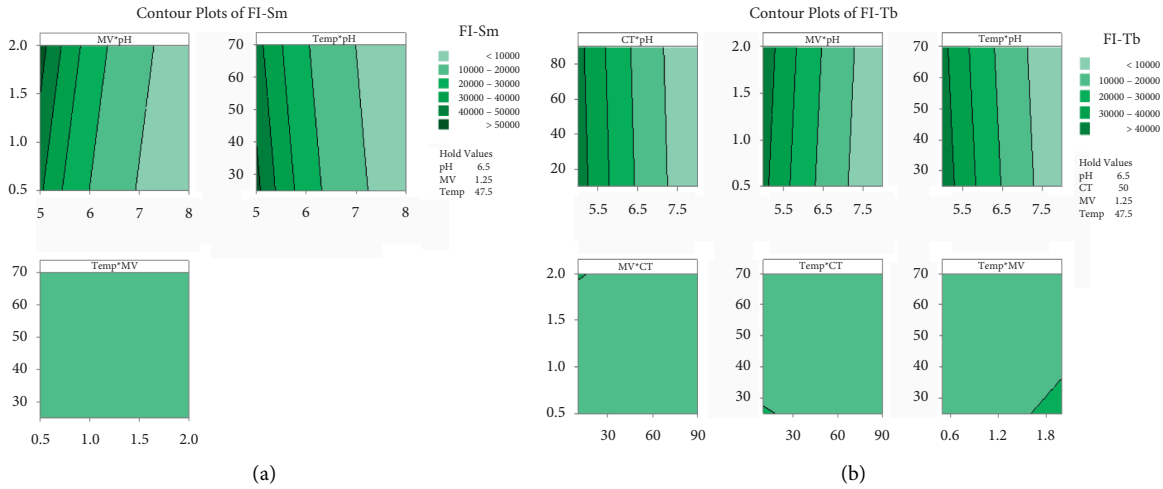

(a) (b)

Figure 4: Two-dimensional contour plots for both ORLX-Sm(III) (a) and ORLX-Tb(III) (b).

Table 4: FT-IR peak assignment for ORLX, ORLX-Sm(III), and ORLX-Tb(III) complexes.

	ORLX	ORLX-Sm(III)	ORLX-Tb(III)	Assignment
Absorption (cm^{-1})	3427	3280	3300	O-H stretching and secondary amine N-H stretching
	2766	2817	2818	C-H stretching for an alkene
	2691	2738	2735	C-H stretching for an alkane
	1643	1613	1614	C=O stretching
	1566	1577	1577	Cyclic alkene C=C stretching
	1458	1472	1473	Methyl group C-H bending
	1363	1389	1389	Carboxylic O-H bending
	1278	1295	1295	C-N stretching
	1053	1056	1062	C-O stretching
	827	827	827	C=C bending

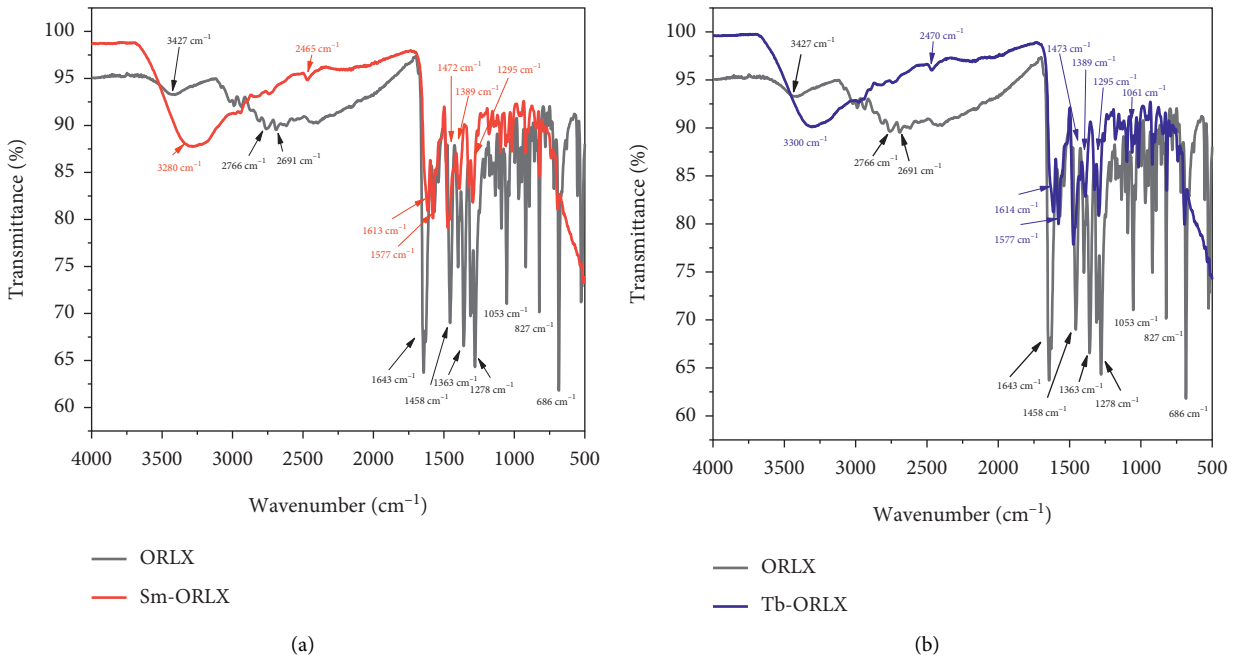

(a) (b)

Figure 5: FT-IR spectrum of ORLX and ORLX-Sm(III) complex (a) and ORLX and ORLX-Tb(III) complex (b).

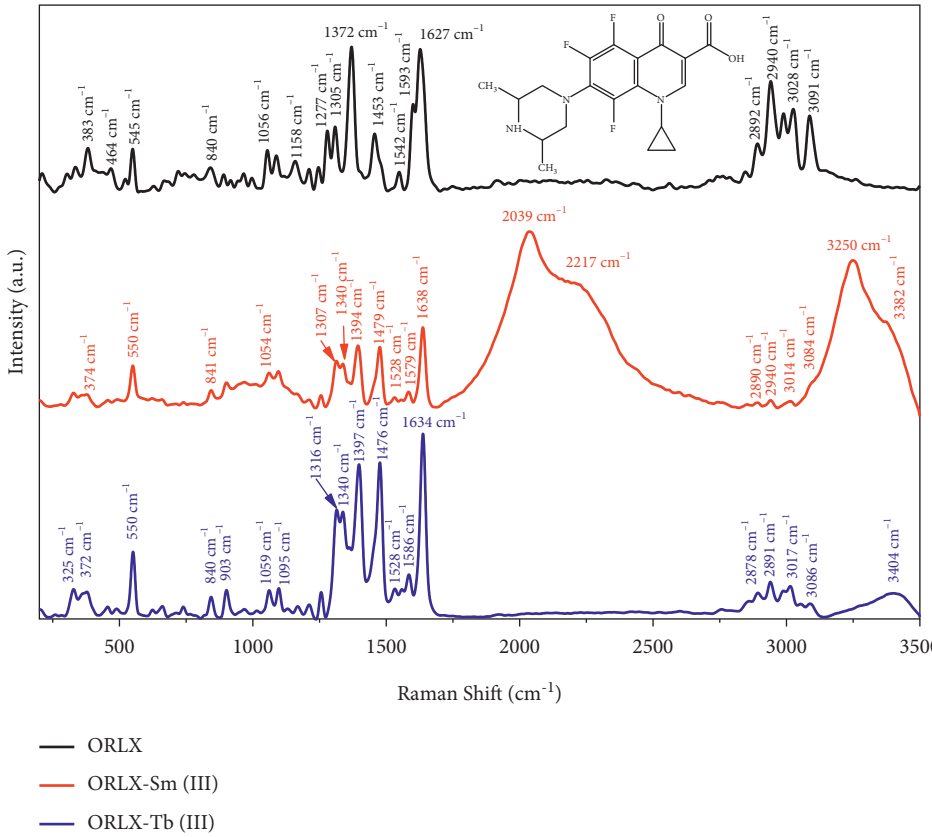

Figure 6: Raman spectra of ORLX, ORLX-Sm(III), and ORLX-Tb(III) complexes.

Table 5: CHN elemental analysis of ORLX, ORLX-Sm(III), and ORLX-Tb(III) complexes.

Compound	C%	H%	N%
ORLX	56.48	5.52	10.35
ORLX-Sm(III)	25.63	3.42	4.71
ORLX-Tb(III)	25.66	3.34	4.64

3.3.4. Determination of the Reaction Stoichiometry and Proposed Complex Structure. Job's method of continuous variation [31] was used to determine the stoichiometric ratio of the reaction between the studied drug ORLX and both metal ions, Sm(III) and Tb(III). The obtained plot showed a maximum value at an ORLX mole fraction of nearly 0.52 in the case of ORLX-Sm(III) and 0.46 for ORLX-Tb(III), indicating the formation of 1 : 1 complex, ORLX : Sm(III) and Tb(III). The structure of the formed complex can be proposed based on the obtained data from the stoichiometric ratio and the FT-IR and Raman analysis as shown in Figure 7 where the metal ion can be coordinated with the drug through two carbonyl functional groups or the carboxylic acid group.

3.4. Method Validation. Validation procedure was performed in accordance with the ICH guidelines [31]. The validated parameters were linearity, sensitivity, selectivity, precision, accuracy, and robustness [43, 44].

3.4.1. Linearity and Range. The general procedure was performed on standard ORLX solutions with increasing concentrations. Calibration curves were obtained by plotting the FI (response) vs. [ORLX-lanthanide chelate] for each solution. The obtained calibration curves were evaluated using linear regression as shown in equations (3) and (4). The calibration curves were linear in the range of 25–500 ng/mL with a coefficient of determination of 0.9997 and 0.9996 for Sm(III) and Tb(III), respectively (Table 6).

$$Y_{\mathrm{OLRX-Sm\,(III)}} = 6.8384x + 38.8509, \quad R^2 = 0.9997, \tag{3}$$

$$Y_{\mathrm{OLRX-Tb\,(III)}} = 6.8159x + 29.5173, \quad R^2 = 0.9996. \tag{4}$$

3.4.2. Sensitivity.

$$\mathrm{LOD} = \frac{3.3\,\mathrm{SD}}{S}, \tag{5}$$

$$\mathrm{LOQ} = \frac{10\mathrm{SD}}{S}. \tag{6}$$

Limit of detection (LOD) and limit of quantification (LOQ) were used to assess the method sensitivity. LOD (S/N ratio = 3) and LOQ (S/N ratio = 10) were calculated using equations (5) and (6), respectively, where SD is the standard deviation of the intercept and S is the slope of the calibration curve. As shown in Table 6, LOD and LOQ were 0.987 and

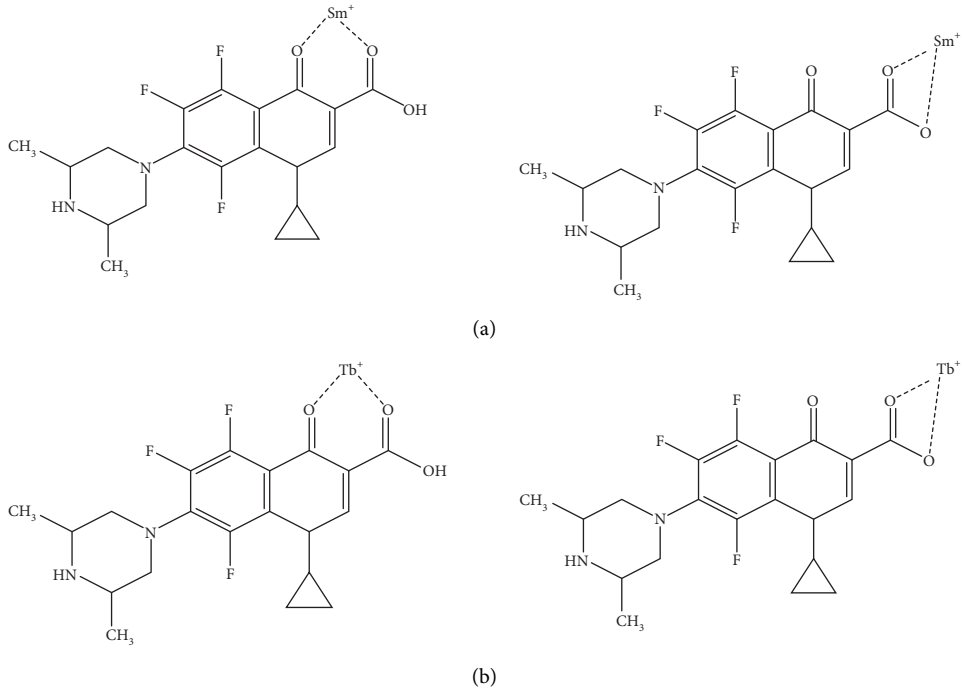

Figure 7: Proposed structure of the ORLX-Sm(III) complex (a) and ORLX and ORLX-Tb(III) complex (b).

Table 6: Analytical parameters for the determination of ORLX via complexation with Sm(III) and Tb(III).

Parameters	ORLX-Sm(III)	ORLX-Tb(III)
λ_{em} (nm)	458	458
Linear range (ng/mL)	25–500	25–500
Regression equation		
Slope (a)	6.8384	6.8159
Intercept (b)	38.8509	−29.5173
Coefficient of determination(R^2)	0.9997	0.9996
LOD (ng/mL)	0.987	1.020
LOQ (ng/mL)	3.289	3.399

3.289 ng/mL for the ORLX-Sm(III) complex and 1.020 and 3.399 ng/mL for the ORLX-Tb(III) complex, respectively. These results reflect the method sensitivity.

3.4.3. Accuracy and Precision. Accuracy and precision were determined at 95.0% confidence interval for 3–7 different concentrations of ORLX as per se. Assessment of the precision was performed three times within the same day (intraday) and on three different days (interday). Results, as revealed in Tables 7 and 8, show good accuracy and precision of the suggested procedure.

3.4.4. Application to the Pharmaceutical Formulation. Method specificity was assessed via application of the proposed procedures to the pharmaceutical formulation. Two procedures were applied: direct calibration method and the standard addition method (Table 9). As shown in Table 9, absence of common interferences from the coformulated materials can be identified from the high % recoveries and low SD values. The estimated % recoveries were in the range of 95–105%, which is in a good match with ICH guidelines.

3.4.5. Ruggedness. PBD, the factorial design selected in the current approach, is well recognized as a ruggedness test. The main reason for choosing PBD as a tool for testing the method ruggedness is that this design focuses mainly on the main effects, where variable-variable interactions are very much confounded with the large main effects [28, 43, 44]. Therefore, the impact of performing slight changes in the process variables on the measured FI as a response was evaluated. For instance, the influence of minor changes in process variables such as pH, Temp, CT, and MV was evaluated. Changes were performed as follows: pH: ±0.5 units, Temp: ±5°C, CT: ±5 min, and MV: ±0.5 mL. The effect of these variations was trivial with RSD% not exceeding 2% in either case. It is crucial to denote that the impact of factorial changes on the FI as a response can also be measured by observing the impact of these variations on the dynamic desirability function plot.

Table 7: Determination of ORLX in the bulk powder using the optimum conditions.

	ORLX-Sm(III)		ORLX-Tb(III)	
Taken (ng/mL)	Found (ng/mL)	% recovery	Found (ng/mL)	% recovery
25.00	24.91	99.64	24.65	98.60
50.00	50.83	101.67	47.44	94.87
100.0	103.92	103.92	101.15	101.15
200.0	193.02	96.51	202.71	101.35
300.0	299.53	99.84	297.41	99.14
400.0	398.63	99.66	405.69	101.42
500.0	501.30	100.26	495.98	99.20
Mean ± SD		100.21 ± 2.25		99.39 ± 2.32
RSD		2.24		2.33

Table 8: Inter- and intraday precision for the determination of ORLX in the bulk powder using the optimum conditions.

ORLX-Sm(III)			ORLX-Tb(III)		
Interday precision					
Concentration (ng/mL)	Mean% recovery ± SD	% error	Concentration (ng/mL)	Mean% recovery ± SD	% error
25.00	100.70 ± 0.30	0.70	25.00	100.70 ± 0.30	0.70
300.0	100.55 ± 0.13	0.55	300.0	100.55 ± 0.13	0.55
500.0	99.92 ± 0.76	0.46	500.0	100.36 ± 0.76	0.46
Intraday precision					
Concentration (ng/mL)	Mean% recovery ± SD	% error	Concentration (ng/mL)	Mean% recovery ± SD	% error
25.00	101.21 ± 2.99	2.71	25.00	101.05 ± 1.40	1.05
200.0	100.95 ± 0.75	0.95	200.0	97.54 ± 0.66	2.46
500.0	99.93 ± 0.69	0.54	400.0	100.40 ± 1.33	0.94

Table 9: Determination of ORLX in the formulation under the optimum conditions. Direct calibration and standard addition methods were performed.

	ORLX-Sm(III)		ORLX-Tb(III)	
Direct calibration method				
Taken (ng/mL)	Found (ng/mL)	% recovery	Found (ng/mL)	% recovery
25.00	24.83	99.31	25.54	102.16
50.00	48.75	97.50	49.15	98.30
100.0	96.40	96.40	100.09	100.09
200.0	208.57	104.29	198.20	99.10
300.0	298.66	99.55	304.27	101.42
400.0	397.78	99.45	397.75	99.44
Mean ± SD		99.42 ± 2.70		100.09 ± 1.46
RSD	2.72	1.46		
Standard addition method				
Taken (ng/mL)	Added (ng/mL)	% recovery	Added (ng/mL)	% recovery
100.0	—	95.64	—	96.67
100.0	50	96.26	50	102.76
100.0	100	100.37	100	103.99
100.0	150	99.24	150	98.87
100.0	200	102.16	200	97.22
100.0	250	100.15	250	101.69
100.0	300	98.97	300	100.88
Mean ± SD		99.64 ± 2.16		100.91 ± 2.79
RSD		2.17		2.77

4. Conclusion

The interaction of Sm(III) and Tb(III) with ORLX produced a complex with high fluorescence. This reaction was implemented for the development of a sensitive, simple, and selective fluorescent-based sensor for the determination of ORLX as per se and in formulation with good recovery. Investigation and optimization of the variables affecting the measured FI were executed using a multivariate approach, PBD, with a desirability function tool for optimization. Results showed that both complexes were significantly affected by pH. On the contrary, CT was the least significant factor in case of the ORLX-Tb(III) complex and had no effect in the case of the ORLX-Sm(III) complex. The

optimization plot showed that the optimum conditions for both complexes that could achieve the maximum FI were pH 5.0, MV 2.0 mL, Temp 25°C, and CT 10 min. Characterization of the solid complexes was performed using FT-IR and Raman analyses, and the obtained data revealed shifting in some peaks confirming the complexation and formation of complexes with similar coordination structures. The reaction stoichiometry for both Sm(III) and Tb(III) with ORLX was determined using Job's methods, and it was found to be 1 : 1 (ORLX : metal ion). Validation of the developed procedure was performed using the ICH guidelines. No effect on the method performance was encountered due to the common additives. Additionally, the procedure is sensitive, selective, facile, and neither time- nor resource-consuming; therefore, it could be suitable for routine quality control analysis of ORLX.

Data Availability

The data used to support the findings of this study are included within the article.

Conflicts of Interest

The authors declare no conflicts of interest.

References

[1] A. C. Alder, A. Bruchet, M. Carballa et al., "Consumption and occurrence," in *Human Pharmaceuticals, Hormones and Fragrances-The Challenge of Micropollutants in Urban Water Management*, T. A. Ternes and A. Joss, Eds., pp. 15–54, IWA Publishing, London, UK, 2006.

[2] S. Rodriguez-Mozaz, I. Vaz-Moreira, S. Varela Della Giustina et al., "Antibiotic residues in final effluents of European wastewater treatment plants and their impact on the aquatic environment," *Environment International*, vol. 140, Article ID 105733, 2020.

[3] K. Kümmerer, "Antibiotics in the aquatic environment-a review-Part I," *Chemosphere*, vol. 75, no. 4, pp. 417–434, 2009.

[4] M. El-Azazy, A. S. El-Shafie, S. Al-Meer, and K. A. Al-Saad, "Eco-structured adsorptive removal of tigecycline from wastewater: date pits' biochar versus the magnetic biochar," *Nanomaterials*, vol. 11, no. 1, p. 30, 2021.

[5] S. K. Cox, "Allometric scaling of marbofloxacin, moxifloxacin, danofloxacin and difloxacin pharmacokinetics: a retrospective analysis," *Journal of Veterinary Pharmacology and Therapeutics*, vol. 30, no. 5, pp. 381–386, 2007.

[6] G.-F. Zhang, S. Zhang, B. Pan, X. Liu, and L.-S. Feng, "4-Quinolone derivatives and their activities against Gram positive pathogens," *European Journal of Medicinal Chemistry*, vol. 143, pp. 710–723, 2018.

[7] P. Dhiman, N. Arora, P. V. Thanikachalam, and V. Monga, "Recent advances in the synthetic and medicinal perspective of quinolones: a review," *Bioorganic Chemistry*, vol. 92, Article ID 103291, 2019.

[8] M. El-Azazy, A. S. El-Shafie, A. Elgendy, A. A. Issa, S. Al-Meer, and K. A. Al-Saad, "A comparison between different agro-wastes and carbon nanotubes for removal of sarafloxacin from wastewater: kinetics and equilibrium studies," *Molecules*, vol. 25, no. 22, p. 5429, 2020.

[9] E. C. L. Cazedey and H. R. N. Salgado, "Orbifloxacin: a review of properties, its antibacterial activities, pharmacokinetic/pharmacodynamic characteristics, therapeutic use, and analytical methods," *Critical Reviews in Analytical Chemistry*, vol. 43, no. 2, pp. 79–99, 2013.

[10] E. Heinen, "Comparative serum pharmacokinetics of the fluoroquinolones enrofloxacin, difloxacin, marbofloxacin, and orbifloxacin in dogs after single oral administration," *Journal of Veterinary Pharmacology and Therapeutics*, vol. 25, no. 1, pp. 1–5, 2002.

[11] J. L. Davis, M. G. Papich, and A. Weingarten, "The pharmacokinetics of orbifloxacin in the horse following oral and intravenous administration," *Journal of Veterinary Pharmacology and Therapeutics*, vol. 29, no. 3, pp. 191–197, 2006.

[12] K. He, A. D. Soares, H. Adejumo, M. McDiarmid, K. Squibb, and L. Blaney, "Detection of a wide variety of human and veterinary fluoroquinolone antibiotics in municipal wastewater and wastewater-impacted surface water," *Journal of Pharmaceutical and Biomedical Analysis*, vol. 106, pp. 136–143, 2015.

[13] T. Morimura, T. Ohno, H. Matsukura, and Y. Nobuhara, "Degradation kinetics of the new antibacterial fluoroquinolone derivative, orbifloxacin, in aqueous solution," *Chemical and Pharmaceutical Bulletin*, vol. 43, no. 6, pp. 1052–1054, 1995.

[14] T. Morimura, Y. Nobuhara, and H. Matsukura, "Photodegradation products of a new antibacterial fluoroquinolone derivative, orbifloxacin, in aqueous solution," *Chemical and Pharmaceutical Bulletin*, vol. 45, no. 2, pp. 373–377, 1997.

[15] M. A. Garcia, C. Solans, J. J. Aramayona, S. Rueda, and M. A. Bregante, "Determination of orbifloxacin in rabbit plasma by high-performance liquid chromatography with fluorescence detection," *Journal of Chromatographic Science*, vol. 37, no. 6, pp. 199–202, 1999.

[16] M. J. Schneider and D. J. Donoghue, "Multiresidue analysis of fluoroquinolone antibiotics in chicken tissue using liquid chromatography-fluorescence-multiple mass spectrometry," *Journal of Chromatography B*, vol. 780, no. 1, pp. 83–92, 2002.

[17] M. J. Schneider and D. J. Donoghue, "Multiresidue determination of fluoroquinolone antibiotics in eggs using liquid chromatography-fluorescence-mass spectrometryn," *Analytica Chimica Acta*, vol. 483, no. 1-2, pp. 39–49, 2003.

[18] L. Johnston, L. Mackay, and M. Croft, "Determination of quinolones and fluoroquinolones in fish tissue and seafood by high-performance liquid chromatography with electrospray ionisation tandem mass spectrometric detection," *Journal of Chromatography A*, vol. 982, no. 1, pp. 97–109, 2002.

[19] E. J. Llorent-Martínez, P. Ortega-Barrales, A. Molina-Díaz, and A. Ruiz-Medina, "Implementation of terbium-sensitized luminescence in sequential-injection analysis for automatic analysis of orbifloxacin," *Analytical and Bioanalytical Chemistry*, vol. 392, no. 7-8, pp. 1397–1403, 2008.

[20] J. M. Traviesa-Alvarez, J. M. Costa-Fernández, R. Pereiro, and A. Sanz-Medel, "Direct screening of tetracyclines in water and bovine milk using room temperature phosphorescence detection," *Analytica Chimica Acta*, vol. 589, no. 1, pp. 51–58, 2007.

[21] S. M. Z. Al-Kindy, K. Al-Shamalani, F. O. Suliman, and H. A. J. Al-Lawati, "Terbium sensitized luminescence for the determination of fexofenadine in pharmaceutical formulations," *Arabian Journal of Chemistry*, vol. 12, no. 8, pp. 2457–2463, 2019.

[22] L. Wang, C. Guo, Z. Chu, and W. Jiang, "Luminescence enhancement effect for the determination of balofloxacin with

balofloxacin-europium (III)-sodium dodecylbenzene sulfonate system," *Journal of Luminescence*, vol. 129, no. 1, pp. 90–94, 2009.

[23] M. A. Omar, M. A. Hammad, and M. Awad, "Utility of Europium ion characteristic peak for quantitation of Fenoterol hydrobromide and Salmeterol xinafoate in different matrices; application to stability studies," *Spectrochimica Acta Part A: Molecular and Biomolecular Spectroscopy*, vol. 217, pp. 182–189, 2019.

[24] S. M. Derayea, A. A. Hamad, D. M. Nagy, D. A. Nour-Eldeen, H. R. H. Ali, and R. Ali, "Improved spectrofluorimetric determination of mebendazole, a benzimidazole anthelmintic drug, through complex formation with lanthanum (III); Application to pharmaceutical preparations and human plasma," *Journal of Molecular Liquids*, vol. 272, pp. 337–343, 2018.

[25] J.-C. G. Bünzli and C. Piguet, "Taking advantage of luminescent lanthanide ions," *Chemical Society Reviews*, vol. 34, no. 12, p. 1048, 2005.

[26] G. Bao, "Lanthanide complexes for drug delivery and therapeutics," *Journal of Luminescence*, vol. 228, Article ID 117622, 2020.

[27] T. Liang, Q. Wang, Z. Li et al., "Removing the obstacle of dye-sensitized upconversion luminescence in aqueous phase to achieve high-contrast deep imaging in vivo," *Advanced Functional Materials*, vol. 30, no. 16, Article ID 1910765, 2020.

[28] M. S. Elazazy, "Factorial design and machine learning strategies: impacts on pharmaceutical analysis," in *Spectroscopic Analyses—Developments and Applications*, E. Sharmin and F. Zafar, Eds., IntechOpen, London, UK, pp. 213–230, 2017.

[29] A. S. El-Shafie, A. W. Khashan, Y. H. A. Hussein, and M. El-Azazy, "Application of a definitive screening design for the synthesis of a charge-transfer complex of sparfloxacin with tetracyanoethylene: spectroscopic, thermodynamic, kinetics, and DFT computational studies," *RSC Advances*, vol. 9, no. 43, pp. 24722–24732, 2019.

[30] M. S. Elazazy and A. A. Shalaby, "Validated spectrophotometric assay of cefepime hydrochloride and cefuroxime sodium using a tetrazolium salt," *E-Journal of Chemistry*, vol. 9, no. 4, pp. 2261–2267, 2012.

[31] I. C. O. Harmonization, *Topic Q2 (R1) Validation of Analytical Procedures: Text and Methodology*, 2005.

[32] P. Job, "Formation and stability of inorganic complexes in solution," *Annali di Chimica*, vol. 9, pp. 113–203, 1928.

[33] Y. Ning, M. Zhu, and J.-L. Zhang, "Near-infrared (NIR) lanthanide molecular probes for bioimaging and biosensing," *Coordination Chemistry Reviews*, vol. 399, Article ID 213028, 2019.

[34] Y. Wang, L. Feng, and C. Jiang, "Fluorimetric study of the interaction between human serum albumin and quinolones-terbium complex and its application," *Spectrochimica Acta Part A: Molecular and Biomolecular Spectroscopy*, vol. 61, no. 13-14, pp. 2909–2914, 2005.

[35] G. E. P. Box and D. R. Cox, "An analysis of transformations," *Journal of the Royal Statistical Society: Series B*, vol. 26, no. 2, pp. 211–243, 1964.

[36] J. Yan, Y. Yu, B. Kong, and S. Zhao, "Highly sensitive detection of sulfasalazine based on the fluorescence quenching of a terbium complex probe," *Microchemical Journal*, vol. 154, Article ID 104553, 2020.

[37] M. El-Azazy, A. S. El-Shafie, and H. Morsy, "Biochar of spent coffee grounds as per Se and impregnated with TiO2: promising waste-derived adsorbents for balofloxacin," *Molecules*, vol. 26, no. 8, p. 2295, 2021.

[38] M. Bakiler, O. Bolukbasi, and A. Yilmaz, "An experimental and theoretical study of vibrational spectra of picolinamide, nicotinamide, and isonicotinamide," *Journal of Molecular Structure*, vol. 826, no. 1, pp. 6–16, 2007.

[39] J. G. Wu, *Modern Fourier Transform Spectroscopic Techniques and its Applications*, pp. 159–186, Science and Technology References Press, Beijing, 1994.

[40] M. Daescu, A. Matea, C. Negrila, C. Serbschi, A. C. Ion, and M. Baibarac, "Photoluminescence as a valuable tool in the optical characterization of acetaminophen and the monitoring of its photodegradation reactions," *Molecules*, vol. 25, no. 19, p. 4571, 2020.

[41] L. Yang, J. Wu, Q. Zhou et al., "Far infrared spectroscopic characterization of sugars and their metal complexes," in *Progress in Fourier Transform Spectroscopy*, J. Mink, G. Keresztury, and R. Kellner, Eds., Springer, Vienna, Austria, pp. 251-252, 1997.

[42] J.-H. Xue, X.-H. Hua, L.-M. Yang et al., "Synthesis, crystal structures and luminescence properties of europium and terbium picolinamide complexes," *Chinese Chemical Letters*, vol. 25, no. 6, pp. 887–891, 2014.

[43] M. S. El-Azazy, "Analytical calibrations: schemes, manuals, and metrological deliberations," in *Calibration and Validation of Analytical Methods - A Sampling of Current Approaches*, M. T. Stauffer, Ed., IntechOpen, London, UK, 2017.

[44] Y. Vander Heyden, K. Luypaert, C. Hartmann, D. L. Massart, J. Hoogmartens, and J. De Beer, "Ruggedness tests on the high-performance liquid chromatography assay of the United States Pharmacopeia XXII for tetracycline hydrochloride. A comparison of experimental designs and statistical interpretations," *Analytica Chimica Acta*, vol. 312, no. 3, pp. 245–262, 1995.